Chapter III

2-photon laser scanning microscopy in the living honeybee

Introduction

The analysis of living tissues with conventional fluorescence microscopy, as shown in Chapters I and II, has some substantial limitations. Spatial resolution and contrast are limited by light scattering, which is due to the inhomogeneities in the refractive index of biological tissues. Since the image quality degrades progressively as one goes deeper in the tissue, high resolution imaging is only possible at the surface. Other major problems are the light induced destruction of fluorophores (photobleaching) and the photodynamic damage of the tissue mediated by the fluorophore or by endogenous chromophores (photodamage). Photobleaching and photodamage cause the deterioration of signal quality and limit the imaging time. These limitations have been largely overcome by 2-photon laser scanning microscopy (2PLSM) (Denk et al., 1990; Denk and Svoboda, 1997).

In conventional fluorescence microscopy fluorophores are excited through single photons which contain the right amount of energy to cause a transition. In 2PLSM, however, fluorophores are excited by the absorption of two low-energy photons which coincide in space in a femtosecond time scale.

Two general features of the 2-photon process are crucial for the high performance of 2PLSM. First, excitation is achieved with long illumination wavelengths because two low-energy photons act together. Compared to the conventional fluorescence technique, which employs 1-photon excitation, light scatters less and penetrates deeper into the tissue. Second, because of the nonlinear dependence of the 2-photon process on light intensity, only fluorophores in the near vicinity of the focal point are excited. Thus a high spatial resolution is achieved both in the lateral (x and y) and vertical (z) directions, avoiding photobleaching and photodamage in the surrounding tissue. Since no fluorescence is generated outside the focal point, all emitted photons,

including the scattered ones, constitute a useful signal and allow efficient signal detection with high spatial and temporal resolutions.

Due to these advantages, 2PLSM offers a wide range of applications for the study of structure and signaling in living tissues (reviewed in Helmchen and Denk, 2002; Brecht et al., 2004).

Several studies have exploited the advantages of this technique in recent years, in particular for functional imaging of dendritic processing and synaptic physiology in brain slices and imaging of individual neuronal processes in the intact brain (Denk et al., 1996; Svoboda et al., 1997; Euler and Denk, 2001; Nimchinsky et al., 2002; Oertner et al., 2002). The combination of 2PLSM with genetically encoded fluorescent proteins is particularly promising, since it solves the problem of labeling specific neurons and leaves the network structure intact. This approach, which is available for Drosophila and mice, has been used for long-term 2PLSM imaging of structural plasticity (Trachtenberg et al., 2002) and to monitor neural activity in the olfactory system (Ng et al., 2002; Wachowiak et al., 2004).

The understanding of neural processes in the honeybee brain would also benefit from functional imaging at high spatial and temporal resolution, and in deeper brain areas. Furthermore, the reduction of photobleaching and photodamage would allow longer lasting imaging experiments. In this chapter I will evaluate the application of 2PLSM to functional imaging in the honeybee.

Materials and Methods

Experiments were performed during a week in June 2002 in Winfried Denk`s laboratory at the MPI für medizinische Forschung, Abt. Biomedizinische Optik, in Heidelberg. Honeybees, *Apis mellifera carnica,* were collected from their hives in our Institute in Berlin and kept in a transportation hive. Bees were prepared as described in Chapter I. Additionally, since 2PLSM is more sensitive to movement artifacts than conventional fluorescence imaging, wing muscles and trachea were removed from the thorax, which was then sealed with low melting point agarose (1.5 % solution; Sigma, A2576). Kenyon cells (KC) were filled with the Ca^{2+} indicators Fura-2 dextran or

Calcium Green-1 dextran (Molecular Probes, Eugene) by injection into the ventral α-lobe of the mushroom body (MB).

Stimulation and imaging

KC activity was evoked either by electrical stimulation of the projection neurons (PN) within the antennal lobe (AL) or by odor stimulation. The AL ipsilateral to the imaged MB was electrically stimulated with a bipolar electrode which provided a current return path that restricted the stimulation to the AL. The electrode consisted of two twisted, isolated silver wires. The wires were superficially inserted in the medial and lateral areas of the AL. Square pulses (10 V, 0.1 ms) were delivered via a stimulus isolation unit (ISO). The following odors were used for olfactory stimulation: 1-hexanol, 2-octanol, limonene, linalool (all from Sigma) and peppermint, orange and clove oil (from the local drugstore). Odors were diluted in mineral oil (see Chapter I) and applied on a piece of filter paper placed in a glass pipette. This pipette was introduced into a glass tube which delivered a constant air stream onto the antennae. For stimulation, air was puffed through the odor containing pipette into the constant air stream. The timing of stimuli was controlled by a stimulus control unit, which also triggered data acquisition.

Images were acquired with a custom built 2PLSM. A mode-locked Ti:Saphire laser (Mira900, 200 fs, 76 MHz, pumped by a 10 W-Verdi laser) was used to illuminate the tissue. The excitation wavelength for both Calcium Green-1 and Fura-2 was 830 ± 15 nm. The laser power was adjusted to 10 - 150 mW (measured at the objective mount) in order to minimize photobleaching and photodamage. Images were acquired through a 40x, 0.8NA W Leica objective (for Figures 3.1, 3.2 and 3.3) or through a 63x, 0.9NA W Zeiss objective (for Figure 3.4). Fluorescence was detected through a dichroic mirror (789 DCSPR) and a 515 ± 25 nm band-pass filter with a photomultiplier tube (Hamamatsu R6357). Image acquisition was controlled by custom written software (CFNT, Bell Laboratories Innovation). The objective was mounted on an x-y-z positioning device (Sutter MP285) to move the objective while keeping the optical path nearly unaffected.

For morphological images the spatial resolution was 256 x 256 pixels (Figures 3.1, 3.2). Image sequences were acquired at different spatial and temporal resolutions. The 2PLSM had a scanning speed of 2 ms per line, thus acquisition rate in line-scan

modus was 500 Hz (Figure 3.3). Images of 64 x 64 pixels were acquired at 7.8 Hz (Figure 3.4).

Data analysis

For morphological images the raw fluorescence images are shown. Ca^{2+} signals were calculated as fluorescence change relative to background fluorescence (ΔF/F). Background fluorescence (F) was determined by the average fluorescence during 200 ms (Figure 3.3) or 1 s (Figure 3.4) before stimulation and was subtracted from every frame of a measurement to give ΔF. No correction or filtering was applied. Note that Fura-2 decreases its fluorescence with increasing Ca^{2+} concentration when excited with the used wavelength. Thus, a negative deflection in the fluorescence represents an increase in the Ca^{2+} concentration. Spatial activity patterns show the averaged ΔF/F of 1 s during odor stimulation (Figure 3.4), signals were inverted and translated into a color code that represents Ca^{2+} increases with warm colors. Signal images were low-pass filtered (3 x 3 pixels) and the lower 20 % was regarded as noise and rejected (Figure 3.4). Dendrites were 3D reconstructed using the Amira 3D software.

Results and Discussion

This first approach to 2PLSM shows that this technique is applicable to honeybees, rendering anatomical and functional high resolution images that allow the analysis of neural function at the level of single dendrites.

Methodological considerations

The first task was to evaluate which of the tested dyes is more suitable to implement the new technique.

Figure 3.1 shows images acquired at different depths in a MB calyx stained with Calcium Green-1. The tissue showed strong background fluorescence and it was not possible to detect dyed dendrites or somata. The calyx neuropil showed a homogenous fluorescence, without visible fibers. Non-fluorescent KC somata were clearly visible in the layers surrounding the neuropil, where they appeared as dark spots in front of a light background, indicating strong fluorescence in the extracellular

space. The high background fluorescence was presumably caused by Calcium Green-1 which diffused into the extracellular space and outshined the labeled KC. Since the extracellular Ca^{2+} concentration is several orders of magnitude higher than the intracellular one, extracellular Calcium Green-1 fluorescence was much higher than the intracellular one. Therefore, mass staining with Calcium Green-1 dextran is apparently not suited for 2PLSM of individual neurons.

However, Figure 3.1 gives some more insights in the potentials and limitations of the 2PLSM approach in insects. Figure 3.1A and B illustrate some effects caused by trachea. The brain surface is covered with a tracheal sack from which air is pumped into the brain tissue via the tracheal tubes. The lower part of this tracheal sack is auto-fluorescent and visible in the 2PLSM images as a corrugated sheet. This sheet is transparent for the laser and does not disturb imaging. However, the air filled tracheal tubes constitute an optical barrier for the laser beam. They appear as fluorescent tubes when in focus (Figure 3.2A), but overshadow the underlying tissue, when above focus. In Figure 3.1A three tracheal tubes, which are just above the focus at a depth of 44 µm, are visible as dark shadows. 24 µm deeper (Figure 3.1B) they still overshadow the tissue. Apart from the problem of overshadowing, thin tracheal tubes can easily be confused with neuronal fibers, when they are in focus and fluoresce. Thus, in order to identify structures as trachea one must check whether their fluorescence turns into a dark shadow, when focusing at a deeper plane.

Figure 3.1 also shows the excellent optical penetration achieved with 2PLSM. At a depth of 197 µm and deeper, axon bundles which run down inside the calyx neuropil (compare with plate 2 in Mobbs, 1982) and type 1 KCs are clearly visible, even though this area is covered by the lip neuropil which is visible at 44 µm. Neural structures were visible up to a depth of 300 µm (data not shown).

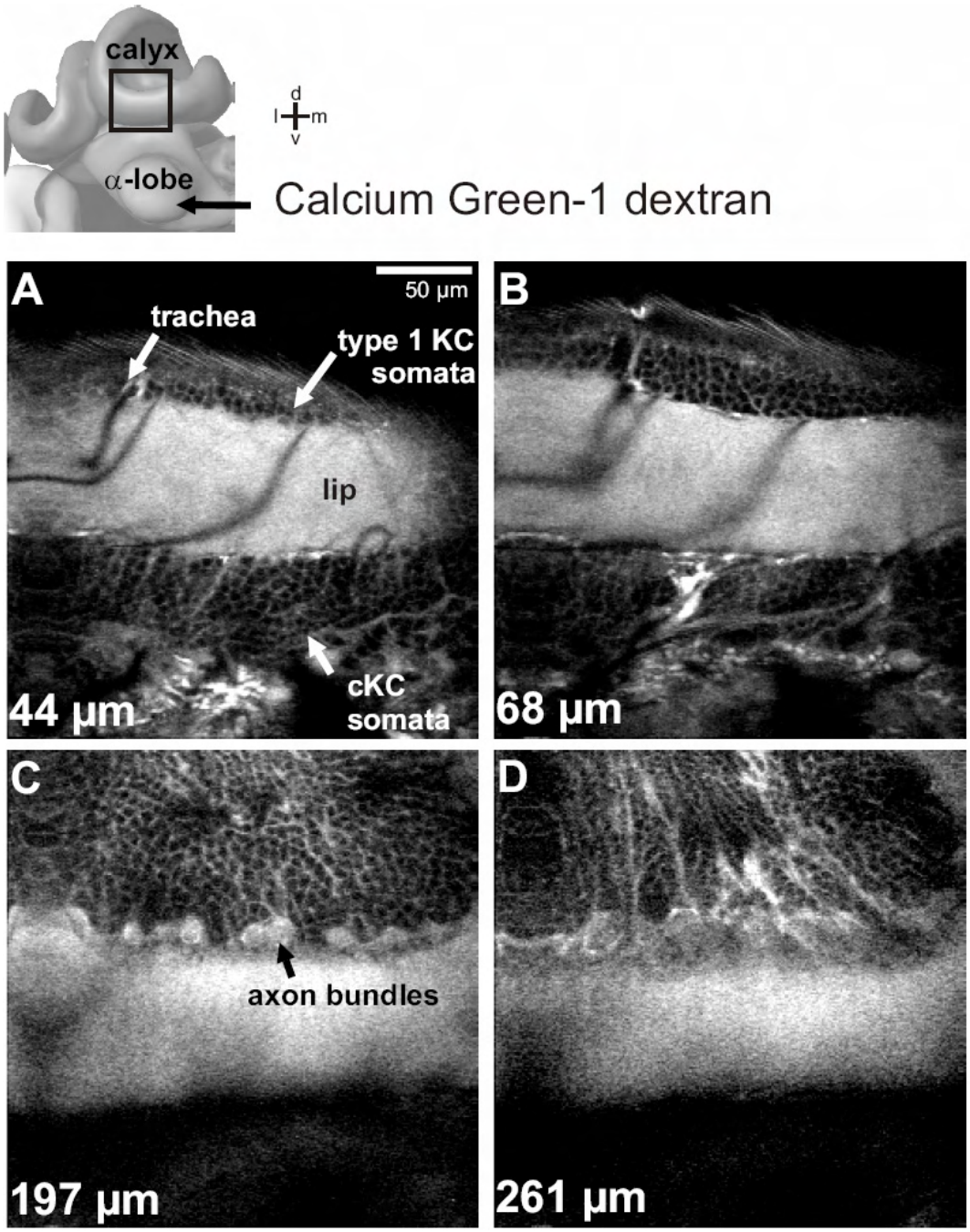

Figure 3.1 Calcium Green-1 staining of the MB calyx

The imaged area covers 250 µm^2 (square in the MB scheme). Calcium Green-1 dextran was injected into the axons of cKCs in the ventral α-lobe (arrow in the scheme). (**A**) The focal plane of the image center lies 44 µm below the brain surface. Due to the curved calyx surface parts of the tracheal sheet (corrugated structure) covering the brain surface are visible. The lip neuropil extends horizontally and shows strong fluorescence. Type 1 KC and cKC somata surround the lip dorsally and ventrally and appear as dark spots in front of a fluorescent background. (**B**) The same area in a depth of 68 µm. (**C**) At a depth of 197 µm the visible neuropil is presumably the collar of the calyx. Axon bundles are visible at the dorsal neuropil border. The focus is below the layer of cKC somata. (**D**) At a depth of 261 µm type 1 KC somata are still visible. The distortion at the left border of the images is due to a synchronization error between the 2PLSM and the acquisition software. d: dorsal, m: medial, l: lateral, v: ventral

To avoid the high background fluorescence caused by Calcium Green-1, Fura-2 was used in the subsequent experiments. At an illumination wavelength of 830 nm, the 2-photon excitation of Fura-2 leads to a fluorescence / [Ca^{2+}] dependency similar to that observed with 1-photon excitation at 380 nm, i.e. Fura-2 shows high fluorescence at low Ca^{2+} concentrations and vice versa. Thus, due to the difference in Ca^{2+} concentration between the intra- and extracellular spaces, Fura-2 shows stronger fluorescence in intracellular compartments. Therefore, extracellularly diffused Fura-2 has less influence on the signal quality than Calcium Green-1 and may be better suited for 2PLSM imaging.

Figure 3.2 shows a Fura-2 staining of the MB calyx. The brain surface (Figure 3.1A) is covered with the corrugated sheet of the tracheal sack. A tracheal opening and a tracheal tube which extends into the lip neuropil are visible. At a depth of 30 µm (Figure 3.1B) the lip neuropil and the surrounding KC soma layers become visible. Compared to the Calcium Green-1 stainings, the background fluorescence was low both in the neuropil and the soma layer and dyed KC somata were clearly visible. Two stained cKC somata were located at 30 µm, while larger groups of somata were visible in 55 and 70 µm (Figures 3.2C and 3.2D). No type 1 KC somata were stained.

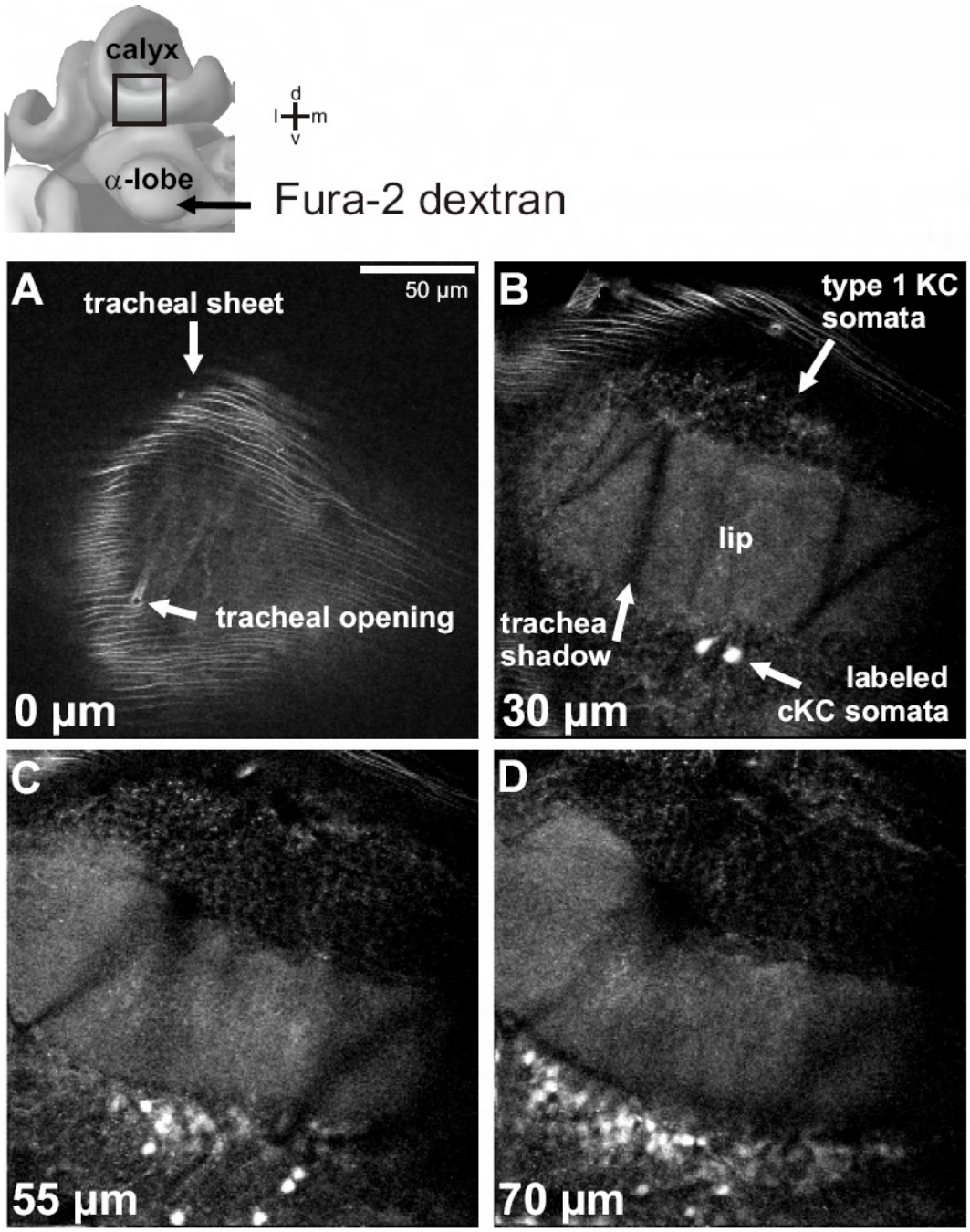

Figure 3.2 Fura-2 staining of the MB calyx

The imaged area covers 210 µm^2. (**A**) The corrugated tracheal sheet which covers the brain is clearly visible. A tracheal tube extends into the neuropil. (**B**) At a depth of 30 µm the lip neuropil and the surrounding KC soma layers become visible. Two labeled cKC are clearly detectable. At 55 µm (**C**) and 70 µm (**D**) different populations of labeled cKC somata appear, however no type 1 KC somata can be seen. d: dorsal, m: medial, l: lateral, v: ventral

Imaging neural activity - Electrically evoked Ca^{2+} signals

In order to record Ca^{2+} signals from KCs, I first stimulated the AL electrically with single 10V pulses which lasted 0.1 ms. PN were activated and excited KCs synaptically.

KC dendrites and somata were imaged at high speed (Figure 3.3) in the line-scan mode, where the laser beam is moved in only one spatial dimension. A line of 64 pixels covering 0.6 x 37 μm^2 was imaged at a rate of 500 Hz. The two upper panels show the raw fluorescence measured over a period of 1280 ms in KC dendrites in the lip, and KC somata. Electrical PN stimulation causes a fast decrease in the fluorescence of the dendrites and a slower one in the KC somata. The time-traces below the panels show the average fluorescence change in an individual dendritic compartment and in a soma. The response delay was ~ 4 ms in the dendrites and ~ 14 ms in the somata. The maximal signal amplitude was reached within ~ 8 ms in the dendrites and within ~ 120 ms in the somata. The magnitude of the signals reached up to 15 % both in the dendrites and somata, and was considerable higher than the signals recorded with conventional fluorescence microscopy (up to 6 % in dendrites and 2.7 % in somata, Chapter I). This difference is presumably due to the low background fluorescence. However, compared to conventional fluorescence microscopy the noise was increased. This can be attributed to the lower number of detected photons in 2PLSM, which leads to an increased shot noise. The different signal kinetics in dendrites and somata may reflect the different surface to volume ratio: small dendrites have a large surface to volume ratio and therefore a fast Ca^{2+} equilibrium while the small surface to volume ratio of the somata results in a slow equilibrium of Ca^{2+} concentration.

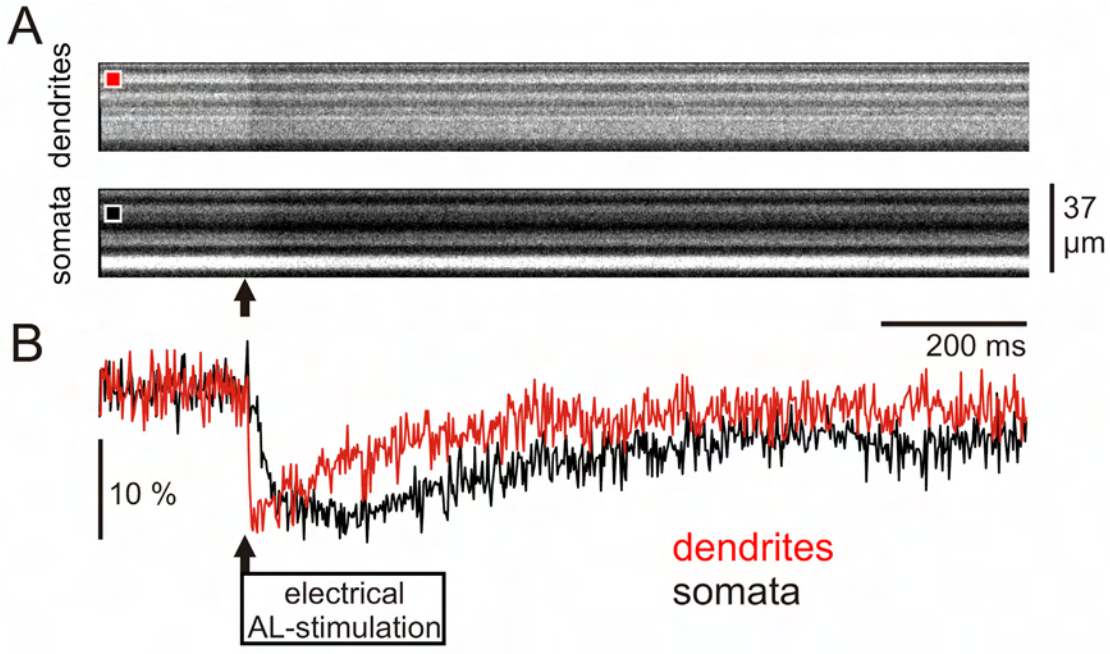

Figure 3.3 Fast Ca^{2+} imaging of KCs

The AL was electrically stimulated (10V, 0.1 ms) in order evoke a PN mediated excitation of KCs. KC dendrites and somata (Fura-2 staining) were recorded in line-scan modus (1 x 64 pixels, 500 Hz). The area covered 0.6 x 37 µm. The upper panels show a single measurement of dendrites and somata during a period of 1280 ms. The imaged lines are aligned horizontally to visualize the change of the fluorescence during stimulation. Light horizontal stripes correspond to dendrites and somata. Dendrites and somata were recorded during two successive stimulation trials. Each recording represents the response to a single stimulation. The time-traces below the panels show the average fluorescence change in 10 pixels, which can be attributed to single dendrite and soma (marked as squares in the upper panels). Note that negative signal deflections represent increases in the Ca^{2+} concentration. Scale bar $\Delta F/F$

Imaging neural activity - Odor evoked Ca^{2+} signals

Finding odor responsive KC somata or dendrites proved to be a difficult task. Odor induced signals were detected in only 2 out-off 18 successful bee preparations. This low efficiency may reflect the low response probability of KCs (Chapter I). Since the z-resolution is extremely high in 2PLSM, signals from only a few KCs are sampled per focal plane. Thus, the chance to find one of the few responding KCs was very low. The sparseness of KC responses does not pose a problem in conventional fluorescence imaging, since signals originating from cells located in different focal planes are collected. In order to facilitate the detection of responding neurons it would be therefore helpful to have an imaging set up that combines 2PLSM with conventional imaging.

Figure 3.4A shows Fura-2 stained dendrites in a depth of 70 µm within the calyx lip. Some of the dendrites responded to odors with a Ca^{2+} increase. Some were activated by 2-octanol and orange, while others responded to orange only.

Figure 3.4B illustrates that movement artifacts are a major problem and its avoidance is an extremely critical point in 2PLSM. The middle image represents the focal plane in which the odor evoked signals were recorded. The other two have been acquired 5 µm below and above of that focal plane. Note that there are considerable differences between those images. Thus, at a spatial resolution which is suited for the imaging of individual dendrites, movement in the µm range causes big artifacts.

Moreover, Figure 3.4 points to the advantage of Ca^{2+} imaging of dendritic compartments and subsequent 3D reconstruction of the imaged structures. Figure 3.4C shows a 3D reconstruction of the area imaged in Figure 3.4A. Such combination of functional imaging data with anatomical data can be used to study mechanisms of dendritic integration.

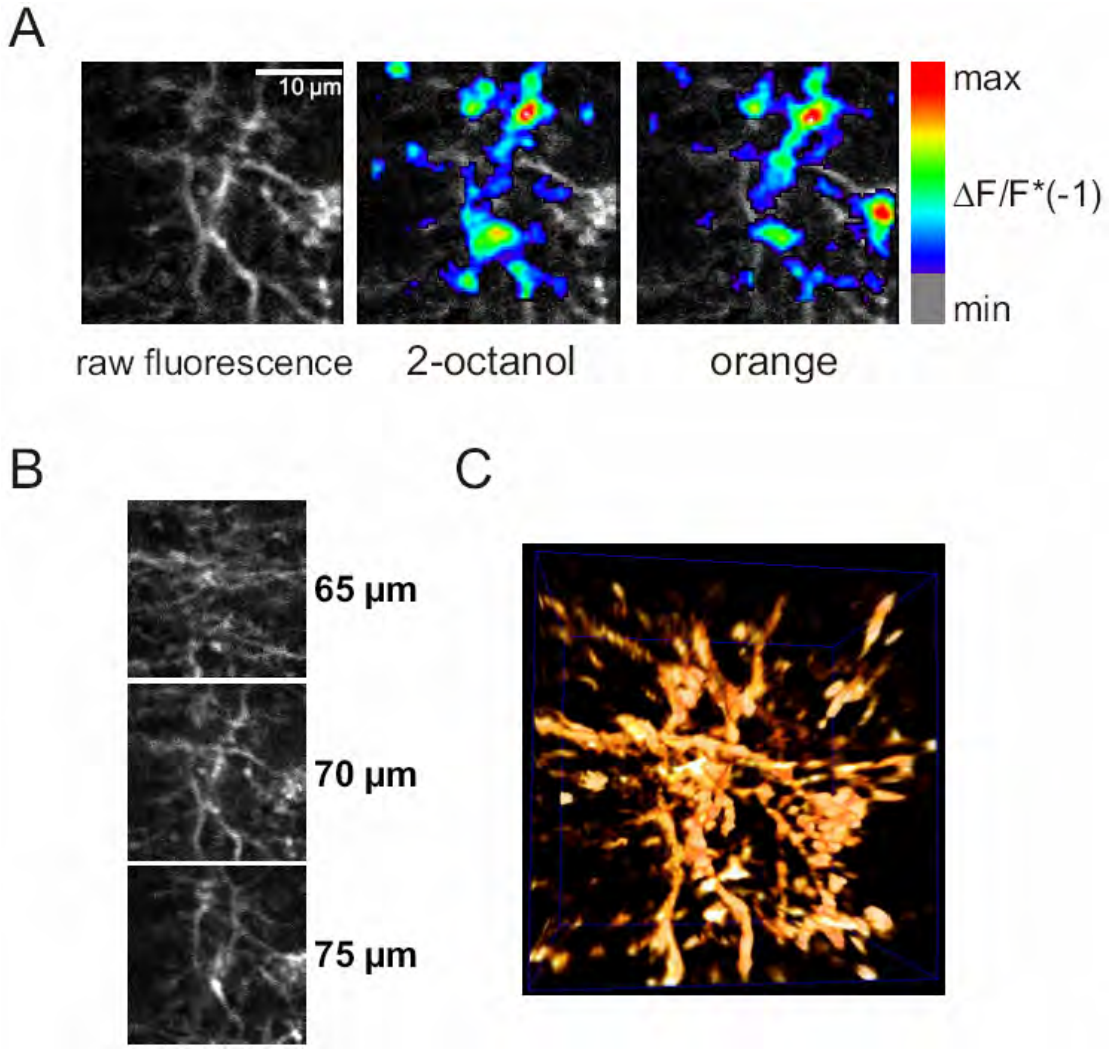

Figure 3.4 High resolution Ca^{2+} imaging of KC dendrites in the lip neuropil

(**A**) Raw fluorescence image of KC dendrites (Fura-2 staining) and color-coded Ca^{2+} signals evoked by stimulation with 2-octanol and orange. Dendrites were located at a depth of 70 µm and the imaged area covered 31 x 31 µm (64 x 64 pixels). (**B**) The same area imaged at a depth of 65, 70 and 75 µm. Note the change in the population of visible dendrites. (**C**) The anatomy of the imaged area was 3D reconstructed from a stack of 20 images (60 to 80 µm) surrounding the imaged plane.

Outlook

The data presented show that 2PLSM can be used to study anatomy and neural signaling at the cellular and subcellular levels in the honeybee brain. Neural structures can be resolved at a depth of up to 300 µm, and the spatial resolution is good enough to visualize individual KC somata and dendritic compartments. Moreover it is possible to record Ca^{2+} signals from KC dendrites and somata at high temporal and spatial resolution. Thus 2PLSM offers an excellent tool to address some of the questions that arise from Chapters I and II and which can not be studied with conventional fluorescence imaging.

The high penetration of 2PLSM could be used, for example, to record from type 1 KCs, which are located inside the calyx, in order to test whether they differ from cKC in their response probabilities or tuning width.

Another great step would be the characterization of the functional relationship between the anatomy of KC dendrites and their integration properties. Functional imaging KC dendrites at high speed followed by high spatial resolution 3D- scanning would provide the basis for detailed models of signal integration.

In order to directly analyze the transmission of odor evoked neural activity from pre- to postsynaptic partners, it would be of great advantage to simultaneously image PN boutons and KCs synaptically connected with them. For that purpose, PNs and KCs should be labeled intracellularly with two dyes that differ in their emission wavelength (for example Calcium Green-1 and Fura-2) and the emitted fluorescence should be guided to two photomultipliers.

Finally, 2PLSM would allow imaging of the bee visual system. So far this has not been possible due to the sensitivity of the honeybee photoreceptors to the excitation light used in conventional microscopy. Since long wavelength laser light is not detected by honeybees' photoreceptors, 2PLSM will provide an excellent tool for the study of the visual system and its integration with other sensory modalities.

Acknowledgments

I am very grateful to Dr. Winfried Denk for giving me the opportunity of testing the bee preparation for 2PLSM in his laboratory. I would also like to thank Dr. Rainer W. Friedrich for his support.

References

Brecht,M., Fee,M.S., Garaschuk,O., Helmchen,F., Margrie,T.W., Svoboda,K., and Osten,P. (2004). Novel approaches to monitor and manipulate single neurons in vivo. J.Neurosci. *24*, 9223-9227.

Denk,W., Strickler,J.H., and Webb,W.W. (1990). Two-photon laser scanning fluorescence microscopy. Science *248*, 73-76.

Denk,W. and Svoboda,K. (1997). Photon upmanship: why multiphoton imaging is more than a gimmick. Neuron *18*, 351-357.

Denk,W., Yuste,R., Svoboda,K., and Tank,D.W. (1996). Imaging calcium dynamics in dendritic spines. Curr.Opin.Neurobiol. *6*, 372-378.

Euler,T. and Denk,W. (2001). Dendritic processing. Curr.Opin.Neurobiol. *11*, 415-422.

Helmchen,F. and Denk,W. (2002). New developments in multiphoton microscopy. Curr.Opin.Neurobiol. *12*, 593-601.

Mobbs,P.G. (1982). The brain of the honeybee Apis mellifera I.The connections and spatial organization of the mushroom bodies. Philosophical Transactions of the Royal Society of London B *298*, 309-354.

Ng,M., Roorda,R.D., Lima,S.Q., Zemelman,B.V., Morcillo,P., and Miesenbock,G. (2002). Transmission of olfactory information between three populations of neurons in the antennal lobe of the fly. Neuron *36*, 463-474.

Nimchinsky,E.A., Sabatini,B.L., and Svoboda,K. (2002). Structure and function of dendritic spines. Annu.Rev.Physiol. *64*, 313-353.

Oertner,T.G., Sabatini,B.L., Nimchinsky,E.A., and Svoboda,K. (2002). Facilitation at single synapses probed with optical quantal analysis. Nat.Neurosci. *5*, 657-664.

Svoboda,K., Denk,W., Kleinfeld,D., and Tank,D.W. (1997). In vivo dendritic calcium dynamics in neocortical pyramidal neurons. Nature *385*, 161-165.

Trachtenberg,J.T., Chen,B.E., Knott,G.W., Feng,G., Sanes,J.R., Welker,E., and Svoboda,K. (2002). Long-term in vivo imaging of experience-dependent synaptic plasticity in adult cortex. Nature *420*, 788-794.

Wachowiak,M., Denk,W., and Friedrich,R.W. (2004). Functional organization of sensory input to the olfactory bulb glomerulus analyzed by two-photon calcium imaging. Proc.Natl.Acad.Sci.U.S.A *101*, 9097-9102.

General Discussion

The aim of this thesis was to understand the principles of odor processing in the MB of the honeybee. Using Ca^{2+} imaging of selectively labeled neurons I found fundamental differences in odor coding between the MB and the AL, and evidence for associative plasticity in the MB intrinsic KCs. These results give novel insights into odor coding and neural plasticity within the MB, and allow conclusions about the interplay of these phenomena in the context of honeybees' odor discrimination and learning capabilities. Furthermore, I developed a preparation that allows the *in vivo* study of anatomy and activity of cellular and subcellular structures in the MB with 2-photon laser scanning microscopy (2PLSM).

In order to explore the function of the MB in odor coding I characterized odor evoked network activity at three consecutive neural compartments (Chapter I). I recorded activity in the dendrites of the PNs that connect the AL with the MB. Next, I recorded the presynaptic terminals of these PNs (boutons). Finally, I characterized their postsynaptic partners, the clawed KCs (cKC). This is the first report showing odor representations at the level of individual PN boutons, and the first characterization of odor specific KC activity in the honeybee.

Both, PN dendrites and boutons exhibited reliable combinatorial patterns of odor evoked activity and showed similar response profiles. However, PN boutons were more narrowly tuned to odors. This sharpening of PN bouton response profiles may be caused by local inhibition within the MB lip through recurrent microcircuits, involving GABAergic neurons (Ganeshina and Menzel, 2001). The next processing step, the transmission from PN boutons to cKCs, is accompanied by further changes in the odor code. Compared to PNs, cKCs responded to odors in a sparser way: individual cKCs were highly odor specific and a given odor activated only a small fraction of the cKC population. cKCs with the same olfactory profile were not grouped into functional subunits as is the case for PNs in the AL glomeruli, but distributed over the MB lip. The sparse odor code found in cKCs is in accordance with findings in locusts and *Drosophila* (Perez-Orive et al., 2002; Wang et al., 2004), and may therefore represent a general property of KCs. Both the distributed nature

and the sparseness of the cKC code may be a result of a divergent-convergent connectivity between PNs and cKCs and a high firing threshold of cKCs (Laurent and Naraghi, 1994; Laurent, 2002; Perez-Orive et al., 2002).

In addition to this transformation in the population code, there was a change in the response dynamic. cKCs transformed the complex temporal pattern of afferent PN activity into brief phasic responses. Remarkably, they integrated PN activity only within the first 200 ms of each response bout. This finding contradicts models proposed by other researchers, which suggest that odor information is encoded in temporal PN activity patterns which develop over hundreds of ms (Laurent and Davidowitz, 1994; Laurent, 1996; Galizia et al., 2000; Stopfer et al., 2003; Fdez et al., 2004; Friedrich and Laurent, 2004). This controversy can only be settled by analyzing the time required by animals to discriminate odors. Ditzen et al. (2003) have shown that honeybees require less than 690 ms to discriminate between any pair of odors. This result is compatible with a temporal coding scheme requiring several hundreds of milliseconds, although the time measured includes both, the time needed for neural processing of odor information and for initiation and execution of behavior. Further results from rats and mice revealed discrimination times of less than 200 ms (Uchida and Mainen, 2003; Abraham et al., 2004). In particular Abraham et al. conclude that increasing odor similarity extends the decision time from 200 ms to around 300 ms. On the one hand, this study supports our finding of fast processing of odor information, but is not in agreement with the invariance in response times for all odors tested in our experiments. This discrepancy could be assigned to differences between the tested species (bees and mice), or could reflect the involvement of other structures in the process of odor discrimination (e.g.: lateral horn in the bee).

The code used by cKCs might be ideally suited for computations underlying odor learning. Each odor is encoded in a combinatorial pattern of simultaneously active cKCs, which is an ideal substrate for associative learning rules of a Hebbian type (Lechner and Byrne, 1998). In order to investigate the role of cKCs in odor learning I conditioned honeybees and simultaneously imaged cKC dendrites in the lip region of the MB calyx (Chapter II). This is the first report of selective KC activity recordings during learning. cKCs responded to the contiguity of odor and sucrose with prolonged and/or increased odor responses. Interestingly, only those cKCs activated by the odor also responded to the reward. This specificity could indicate that the sucrose effect is

mediated by a neuromodulator, rather than by an excitatory neurotransmitter which would recruit otherwise silent cKCs (see Discussion in Chapter II). A possible candidate is octopamine, which could be released by the VUM_{mx1} neuron, a neuron shown to represent the reinforcing function in appetitive odor learning (Hammer, 1993; Hammer and Menzel, 1998).

The results show that associative conditioning does not alter the overall population of cKCs that respond to the rewarded odor. In other words, there is no recruitment of new cKCs into the odor response pattern. However, cKCs showed increased responses to the rewarded relative to the unrewarded odor 15 minutes after training or longer. These changes correspond to the differential changes in response probability typically observed in behavioral experiments (Menzel, 1990). These results suggest that the formation of odor memories depends on the modulation of cKCs' spiking activity, probably through a heterosynaptic mechanism, involving the VUM_{mx1} neuron, causing a strengthening of the PN-KC synapses.

The results from Chapters I and II are integrated in a functional model of the MB (Figure 2.5 in Chapter II). This model suggests a solution to the computational problem of odor learning, exploiting the advantages derived from the coding properties of cKCs. This model proposes that learning is based on two sequential steps and depends on heterosynaptic plasticity in the MB calyx (input area) and on monosynaptic, spike-rate dependent plasticity at the MB lobes (output area), where MB output neurons could be recruited. These neurons would then encode the significance of the learnt odor as reward predictor. Since KCs of different sensory modalities project to the α-lobe, and MB output neurons receive input across the α-lobe, the suggested learning mechanism may not only lead to elementary odor learning but also allow higher-order associations, in particular the embedding of olfactory memories into a multisensory context. Due to the sparse nature of the cKC code, overlaps between individual odor representations are unlikely, and a single MB output neuron could store many odor memories without interference, allowing fine odor discrimination. Odor learning in the MB may, therefore, account for the ability of honeybees to reliably discriminate similar odors (Laska et al., 1999; Ditzen et al., 2003). In many circumstances however, since the composition of food related odors is highly variable, it may be advantageous for an animal to generalize between similar odors (Waser et al., 1996). Therefore the olfactory system should provide learning

mechanisms that allow both, fine odor discrimination and generalization between similar odors. This task may be achieved by distributing the learning mechanisms across different levels of the olfactory system. In the honeybee associative odor learning depends on both the AL and the MB (Hammer and Menzel, 1998; Menzel, 2001). Due to the broadly overlapping response profiles of glomeruli (Chapter I), a learning mechanism which relies on the odor code present in the AL would not be suitable for fine odor discrimination, but would allow generalization between odors that evoke overlapping activity patterns. However, it remains to be tested whether the similarity of glomerular activity patterns indeed correlates with the degree of odor generalization.

References

Abraham,N.M., Spors,H., Carleton,A., Margrie,T.W., Kuner,T., and Schaefer,A.T. (2004). Maintaining accuracy at the expense of speed: stimulus similarity defines odor discrimination time in mice. Neuron *44*, 865-876.

Ditzen,M., Evers,J.F., and Galizia,C.G. (2003). Odor similarity does not influence the time needed for odor processing. Chem.Senses *28*, 781-789.

Fdez,G.R., Sachse,S., Galizia,C.G., and Herz,A.V. (2004). Odor-driven attractor dynamics in the antennal lobe allow for simple and rapid olfactory pattern classification. Neural Comput. *16*, 999-1012.

Friedrich,R.W. and Laurent,G. (2004). Dynamics of olfactory bulb input and output activity during odor stimulation in zebrafish. J.Neurophysiol. *91*, 2658-2669.

Galizia,C.G., Kuttner,A., Joerges,J., and Menzel,R. (2000). Odour representation in honeybee olfactory glomeruli shows slow temporal dynamics: an optical recording study using a voltage-sensitive dye. J.Insect Physiol *46*, 877-886.

Ganeshina,O. and Menzel,R. (2001). GABA-immunoreactive neurons in the mushroom bodies of the honeybee: an electron microscopic study. J.Comp Neurol. *437*, 335-349.

Hammer,M. (1993). An identified neuron mediates the unconditioned stimulus in associative olfactory learning in honeybees. Nature *366*, 59-63.

Hammer,M. and Menzel,R. (1998). Multiple sites of associative odor learning as revealed by local brain microinjections of octopamine in honeybees. Learn.Mem. *5*, 146-156.

Laska,M., Galizia,C.G., Giurfa,M., and Menzel,R. (1999). Olfactory discrimination ability and odor structure-activity relationships in honeybees. Chem.Senses *24*, 429-438.

Laurent,G. (1996). Dynamical representation of odors by oscillating and evolving neural assemblies. Trends Neurosci. *19*, 489-496.

Laurent,G. (2002). Olfactory network dynamics and the coding of multidimensional signals. Nat.Rev.Neurosci. *3*, 884-895.

Laurent,G. and Naraghi,M. (1994). Odorant-induced oscillations in the mushroom bodies of the locust. J.Neurosci. *14*, 2993-3004.

Laurent,G.J. and Davidowitz,H. (1994). Encoding of olfactory information with oscillating neural assemblies. Science *265*, 1872-1875.

Lechner,H.A. and Byrne,J.H. (1998). New perspectives on classical conditioning: a synthesis of Hebbian and non-Hebbian mechanisms. Neuron *20*, 355-358.

Menzel,R. (1990). Learning, memory, and "cognition" in honey bees. In Neurobiology of comparative cognition, R. P. Kesner and D. S. Olton, eds. (Hillsdale, N.J.: Erlbaum Inc.), pp. 237-292.

Menzel,R. (2001). Searching for the memory trace in a mini-brain, the honeybee. Learn.Mem. *8*, 53-62.

Perez-Orive,J., Mazor,O., Turner,G.C., Cassenaer,S., Wilson,R.I., and Laurent,G. (2002). Oscillations and sparsening of odor representations in the mushroom body. Science *297*, 359-365.

Stopfer,M., Jayaraman,V., and Laurent,G. (2003). Intensity versus identity coding in an olfactory system. Neuron *39*, 991-1004.

Uchida,N. and Mainen,Z.F. (2003). Speed and accuracy of olfactory discrimination in the rat. Nat.Neurosci. *6*, 1224-1229.

Wang,Y., Guo,H.F., Pologruto,T.A., Hannan,F., Hakker,I., Svoboda,K., and Zhong,Y. (2004). Stereotyped odor-evoked activity in the mushroom body of Drosophila revealed by green fluorescent protein-based Ca2+ imaging. J.Neurosci. *24*, 6507-6514.

Waser,N.M., Chittka,L., Price,M.V., Williams,N.M., and Ollerton,J. (1996). Generalization in pollination systems, and why it matters. Ecology *77*, 1043-1060.